Atomic Spectroscopy

Article

Assessing Apatite Reference Materials and Common Pb Correction for in Situ U–Pb Geochronology

Fen Xiao,[a,b] Yueheng Yang,[a,b,*] Lei Xu,[a,b] Shitou Wu,[a,b] Chao Huang,[a,b] Hao Wang,[a,b] Liewen Xie,[a,b] Jinhui Yang,[a,b] and Fuyuan Wu[a,b]

[a] State Key Laboratory of Lithospheric and Environmental Coevolution, Institute of Geology and Geophysics, Chinese Academy of Sciences, Beijing 100029, P. R. China

[b] College of Earth and Planetary Science, University of Chinese Academy of Sciences, Beijing 100049, P. R. China

Received: *February 09, 2026;* ***Revised:*** *March 10, 2026;* ***Accepted:*** *March 12, 2026;* ***Available online:*** *March 12, 2026.*

DOI: 10.46770/AS.2026.026

ABSTRACT: Apatite is a common accessory mineral in U–Pb geochronology and provides valuable constraints on magmatic evolution, orogenic processes, and basin thermal histories. However, its generally low U concentrations and high common Pb contents have limited its broader application. The long-term stability of matrix-matched reference materials and the reliability of common Pb correction are critical factors controlling data quality. Here, we present in situ U–Pb data obtained by LA–SF–ICP–MS for a suite of widely used apatite reference materials, including NW-1, McClure Mountain, Emerald, Durango, Otter Lake, MAD, AP1 and AP2, covering an age range from ~1157 to 32 Ma. Their long-term stability and homogeneity are evaluated based on analytical results over the past five years. Using real reference materials with contrasting common Pb contents, we further assess the influence of common Pb correction using anchored initial Pb compositions with propagated uncertainties. The results show that U–Pb ages for most reference materials are consistent with ID–TIMS certified values or previously published data, with deviations ≤2%, demonstrating their long-term analytical stability. NW-1, characterized by high U concentrations and the lowest common Pb, is recommended as primary reference material, whereas AP1 and AP2 are better suited as secondary reference materials. This study confirms the robustness of the established analytical protocol, clarifies the appropriate application of different apatite reference materials, and provides a practical framework for matrix matching and multi–reference material cross-calibration in in situ apatite U–Pb geochronology.

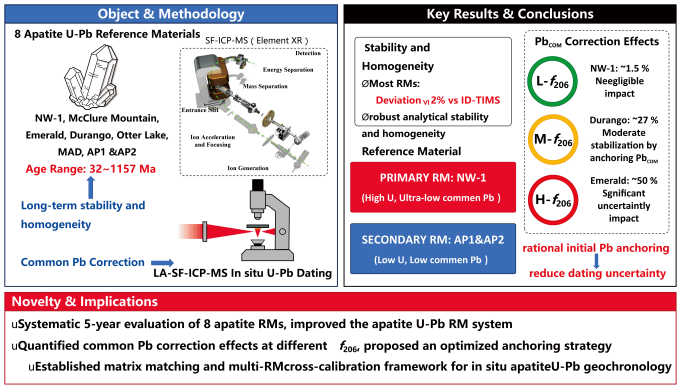

INTRODUCTION

Apatite [$Ca_5(PO_4)_3(F, Cl, OH)$] is a ubiquitous accessory mineral occurring in nearly all major rock types. Owing to its relatively high closure temperature (450–550 °C)[1] and its ability to incorporate radioactive elements such as U, apatite has become an important target in geochronological studies. U–Pb geochronology of apatite provides critical constraints on magmatic evolution and provenance, while apatite fission-track thermochronology has been widely applied to investigations of basin thermal histories, orogenic evolution, and landscape development.

Although isotope dilution–thermal ionization mass spectrometry (ID–TIMS) offers very high analytical precision [2,3], it is fully destructive and labor intensive. In contrast, secondary ion mass spectrometry (SIMS) and laser ablation inductively coupled plasma mass spectrometry (LA-ICP-MS) offer distinct advantages, including simpler sample preparation, minimal sample damage, and high spatial resolution and analytical throughput.[4-12] As a result, in situ analytical techniques have become the preferred approaches for apatite U–Pb dating.

Reliable in situ microanalysis requires effective correction for instrumental mass fractionation and drift, as well as the use of appropriate matrix-matched reference materials[4-7,13]. Since the early 21st century, advances in instrumentation and analytical protocols have led to a rapid expansion in apatite U–Pb geochronology[4,5,7,9,14,15]. Correspondingly, apatite reference materials have evolved from a single early standard to a more comprehensive system covering a wide range of ages and analytical techniques. However, the long-term stability and homogeneity of some commonly used reference materials remain insufficiently evaluated.

In addition, apatite typically contains low U concentrations and limited radiogenic Pb, particularly in young samples, which poses significant challenges for precise U–Pb dating. The ubiquitous presence of common Pb in apatite—including in reference materials—represents a major limitation for in situ U–Pb analyses[4-7,9,16,17]. Although the Sr and Nd isotopic compositions of several apatite U–Pb reference materials have previously been characterized using solution and laser-based techniques[8], systematic evaluation of their U–Pb isotopic stability and common Pb behavior is still required.

In this study, we assess the long-term stability of eight widely used apatite U–Pb reference materials based on LA–SF–ICP–MS analyses conducted in our laboratory over the past five years. Based on their U–Pb isotopic characteristics and common Pb contents, we identify suitable primary and secondary reference materials for matrix-matched correction of elemental fractionation. Using real reference materials with contrasting common Pb contents—NW-1 (~1.5% f_{206}), Durango (~27% f_{206}), and Emerald (~50% f_{206})—we further evaluate the effects of common Pb correction on calculated U–Pb ages using anchored initial Pb compositions with propagated uncertainties.

EXPERIMENTAL

All analyses were performed at the State Key Laboratory of Lithospheric and Environmental Coevolution (SKLLEC), Institute of Geology and Geophysics, Chinese Academy of Sciences (IGGCAS), Beijing. Apatite samples used in this study were derived from a variety of rock types ranging in age from the Paleoproterozoic to the Cretaceous. The samples were either provided by collaborating geologists or purchased from mineral collectors. Detailed descriptions of individual apatite samples are presented in the following sections.

Some apatite samples (Otter Lake, MAD, Emerald, Durango, AP1, AP2) contained relatively large grains (up to several millimeters). Grains free of visible inclusions were hand-picked under a binocular microscope. Selected grains were mounted in 1-inch epoxy discs, sectioned to expose their interiors, polished, and photographed. Prior to laser ablation analysis, the mounts were cleaned in 2% HNO_3 for several minutes. Chemical homogeneity of the apatite grains was evaluated by LA-Q-ICP-MS and its Sr-Nd isotopic composition are described in detail elsewhere[8]. U–Pb isotopic homogeneity was further assessed by repeated LA-SF-ICP-MS analyses conducted over the past five years.

In situ U–Pb analysis. In situ U–Pb isotope analyses were carried out using a single-collector sector-field ICP-MS (Element XR, Thermo Fisher Scientific) coupled to a 193 nm ArF excimer laser ablation system (Geolas HD, Coherent) at IGGCAS. The Element XR was equipped with a high-capacity vacuum pump (OnTool Booster 150, Asslar, Germany). Together with a high-performance Jet sample cone, this configuration significantly enhanced signal intensity.[18-20]Helium (~0.75 L min^{-1}) was used as the carrier gas within the ablation cell, with a small addition of nitrogen (6 mL min^{-1}), and subsequently mixed with argon (~0.95 L min^{-1}) downstream of the cell to improve sensitivity for U and Pb isotopes. Detailed instrumental settings are provided in Wu *et al.* [21,22].

Instrument performance was optimized daily using NIST SRM 612 [23].and ARM-3 [24] reference materials. Optimization focused on maximizing signal-to-background ratios for Pb, Th, and U, while maintaining low oxide production ($ThO^+/Th^+ < 0.5\%$), low double-charged ion production ($Ca^{2+}/Ca^+ < 1.0\%$), and stable plasma conditions ($U^+/Th^+ = 0.95–1.05$). The isotopes ^{202}Hg, ^{204}Pb, ^{206}Pb, ^{207}Pb, ^{208}Pb, ^{232}Th, ^{235}U, and ^{238}U were measured by cycling the electrostatic analyzer in E-scan mode at a fixed magnetic field. Dwell times were set to 15 ms for ^{206}Pb and ^{238}U, 2 ms for ^{202}Hg and ^{204}Pb, 10 ms for ^{208}Pb and ^{232}Th, and 30 ms for ^{207}Pb. Typical operating parameters are summarized in Table 1.

Prior to each analytical session, a pre-ablation step was performed to remove surface contamination by ablating a 90 μm spot for five laser pulses. Each spot analysis consisted of approximately 15 s of background acquisition followed by 45 s of signal acquisition.

Data reduction. Raw analytical data were exported for offline processing. Data reduction and age calculations were performed using Iolite 4.0 [25,26]. Tera–Wasserburg (T–W) concordia regressions were conducted using IsoplotR[27]. Signals for ^{204}Pb, ^{206}Pb, ^{207}Pb, ^{208}Pb, ^{232}Th, and ^{238}U were measured. The ^{235}U signal was calculated from ^{238}U using a constant $^{238}U/^{235}U$ ratio of 137.818 [28].

U-Pb age data were processed using the "two–step correction procedure [4,5,13,15,22]. Pb/U fractionation was using the standard-sample bracketing (SSB) method [30]. Instrumental fractionation was first corrected using NIST 612 [23] and ARM-3[24].

Table 1 Typical instrumental parameters for LA-SF-ICP-MS U–Pb dating of apatite

Laser ablation system	
Manufacturer, model and type	Coherent Geolas HD
Ablation cell and aerosol transport volume	Custom-built ablation cell; aerosol transport volume < 3 cm^3
Laser wavelength	193 nm
Energy density / fluence	~3, 4, 5 J/cm^2
Repetition rate	4, 5 Hz
Ablation spot size	32, 44, 60 μm
Sampling mode / method	Single-spot ablation
Ablation gas flow rate	~0.75 L/min (He)
Ablation duration	Variable
ICP-MS system	
Manufacturer, model and type	Thermo Fisher scientific, Element XR
Rf power	1320 W
Guard electrode	Connected (Pt)
Sample cone	Nickel Jet sample cone
Skimmer cone	Nickel X skimmer cone
Carrier gas (Ar) flow rate	0.95 L/min
Enhancement gas N_2) flow rate	6 mL/min
Scan mode	E-scan
Measured isotopes (m/z) and dwell time (ms)	^{202}Hg (2), ^{204}Pb (2), ^{206}Pb (15), ^{207}Pb (30), ^{208}Pb (10), ^{232}Th (10), ^{235}U (10), ^{238}U (15)
Mass window	20%
Number of points per peak	20
Detection system	Single SEM detector (triple mode: counting, analog, faraday cup)
Resolution	Low (~300)
Total integration time per acquisition	0.27 s

Then use matrix-matched apatite reference materials to calculate fractionation correction factor, following the steps below:

(1) The intercept of the discordia line constructed by all measured analyses with the x-axis was determined, the intercept of the discordia line anchored at the recommended age of the reference material with the x-axis was calculated;

(2) The ratio between the two intercepts represents the Pb/U fractionation correction factor;

(3) The corrected $^{206}Pb/^{238}U$ ratio of the unknown sample was obtained by multiplying its measured $^{206}Pb/^{238}U$ ratio by this factor. The $^{207}Pb/^{206}Pb$ ratio was directly corrected using glass reference materials with homogeneous Pb isotopic compositions.

The fractionation-corrected data were plotted on Tera–Wasserburg (T–W) concordia diagrams. All intercept ages in this study were anchored using the ratios calculated from the Stacey and Kramers [29] Pb evolution model, with an uncertainty set at the 2% level.

Apatite containing common Pb typically requires additional common Pb correction [13,15]. In this study, common Pb correction was performed using the ^{207}Pb-based method. The proportion of common ^{206}Pb (f_{206}) was calculated according to the following equation:

$$f_{206} = \frac{(^{207}Pb/^{206}Pb)_{measured} - (^{207}Pb/^{206}Pb)_{rad}}{(^{207}Pb/^{206}Pb)_{common} - (^{207}Pb/^{206}Pb)_{rad}} \quad (1)$$

Where:

$$(^{207}Pb/^{206}Pb)_{rad} = \left(\frac{^{235}U}{^{238}U}\right) \times \frac{e^{\lambda_{235}t} - 1}{e^{\lambda_{238}t} - 1} \quad (2)$$

Where, $(^{207}Pb/^{206}Pb)_{measured}$ refers to the measured $^{207}Pb/^{206}Pb$ ratio of samples; $(^{207}Pb/^{206}Pb)_{common}$ denotes the initial $^{207}Pb/^{206}Pb$ ratio of common Pb, which is estimated using the two-stage crustal Pb evolution model proposed by Stacey and Kramers [29]. In this study, the $^{206}Pb/^{238}U$ ages are the weighted mean ages after common Pb correction.

As multiple datasets from repeated analyses of various samples are presented in this study, the reference materials used for data

Table 2 LA-SF-ICP-MS analytical results of apatite reference materials from 2021 to 2026

Apatite	Session time	No	Intercept U-Pb age (±2s) (Ma)	^{207}Pb corr. $^{206}Pb/^{238}U$ age (±2s) (Ma)	*f 206* mean (%)	Apatite	Session time	No	Intercept U-Pb age (±2s) (Ma)	^{207}Pb corr. $^{206}Pb/^{238}U$ age (±2s) (Ma)	*f 206* mean (%)
S1	2025.10.11	22	1170 ± 12	1164 ± 12	~ 1.5	S5	2017.09.27	23	92.2 ± 1.1	92.2 ± 1.2	~45.6
S2	2024.12.28	26	1172 ± 13	1174 ± 14	~ 1.6	Emerald	mean	107	92.5 ± 0.6	92.9 ± 0.7	
S3	2023.08.24	36	1171 ± 16	1168 ± 33	~ 1.7	S1	2023.07.28	27	32.9 ± 0.7	32.8 ± 0.7	~ 28.2
S4	2022.07.31	34	1148 ± 18	1152 ± 19	~ 0.8	S2	2023.07.28	33	33.1 ± 0.7	33.2 ± 0.7	~ 27.1
S5	2022.07.15	14	1146 ± 23	1147 ± 23	~ 1.6	S3	2023.07.28	20	32.4 ± 0.5	32.4 ± 0.5	~26.2
S6	2021.11.27	26	1145 ± 13	1145 ± 12	~ 1.5	S4	2023.07.28	25	31.7 ± 0.5	31.8 ± 0.5	~25.0
S7	2021.11.26	14	1161 ± 15	1153 ± 15	~ 1.5	Durango	mean	105	32.3 ± 0.6	32.4 ± 0.3	
S8	2021.11.25	24	1151 ± 9	1151 ± 10	~ 1.3	S1	2023.12.21	34	915.1 ± 6.2	914.2 ± 6.2	~ 2.6
NW-1	mean	195	1157 ± 5	1157 ± 4		S2	2023.12.04	18	925.0 ± 9.0	921.0 ± 12.0	~ 2.8
S1	2021.11.27	27	523.7 ± 6.6	523.1 ± 6.0	~ 21.0	Otter Lake	mean	52	916.8 ± 5.2	916.6 ± 5.1	
S2	2021.11.26	14	528.1 ± 7.8	523.9 ± 7.8	~ 22.4	S1	2026.01.31	32	483.2 ± 6.4	480.4 ± 4.0	~ 8.5
S3	2021.11.25	12	534.1 ± 11.1	535.0 ± 12.0	~ 23.5	S2	2017.09.26	25	483.2 ± 6.4	483.2 ± 6.6	~ 8.3
S4	2021.11.25	24	506.8 ± 5.2	506.9 ± 4.6	~ 21.2	MAD	mean	57	482.0 ± 3.1	481.9 ± 2.4	
S5	2017.09.27	13	521.4 ± 5.0	521.0 ± 5.5	~ 15.6	S1	2026.01.31	29	470.0 ± 3.6	469.7 ± 3.5	~ 2.1
McClure M.	mean	90	519.5 ± 2.0	518.8 ± 2.2		S2	2017.09.26	18	476.8 ± 3.5	477.1 ± 7.6	~ 2.5
S1	2025.07.21	24	93.5 ± 2.1	93.5 ± 2.2	~ 49.3	AP1	mean	47	473.2 ± 2.7	473.2 ± 2.6	
S2	2024.12.28	24	100.2 ± 3	99.8 ± 2.6	~55.5	S1	2026.01.31	26	480.3 ± 3.3	480.0 ± 3.3	~ 3.1
S3	2023.12.21	22	91.7 ± 1.6	91.8 ± 1.7	~ 47.5	S2	2017.09.26	23	476.4 ± 2.8	476.3 ± 2.7	~ 3.0
S4	2022.07.14	14	92.0 ± 1.2	92.3 ± 1.5	~ 41.0	AP2	mean	49	477.9 ± 2.2	477.8 ± 2.1	

corrected are specified as follows: All data except those acquired in 2021 were corrected for instrumental fractionation using NIST 612, while the 2021 data used ARM-3. The $^{206}Pb/^{238}U$ ratios of Otter Lake, McClure Mountain, MAD, AP1, and AP2 were corrected using NW-1; The $^{206}Pb/^{238}U$ ratios of NW-1were corrected using Otter Lake; The $^{206}Pb/^{238}U$ ratios of Emerald and Durango were both directly corrected using glass reference materials.

Elemental concentration was quantified using NIST 612 glass as the external standard, which has U contents comparable to apatite. Quantification was achieved using the DRS module in the Iolite software [25,26].

RESULTS

In this study, in situ U–Pb isotopic compositions and ages of eight widely used apatite reference materials (NW-1, McClure Mountain, Emerald, Durango, Otter Lake, MAD, AP1 and AP2) were determined using LA–SF–ICP–MS (Table S1). In addition, long-term replicate analytical data collected over the past five years for four of these reference materials (NW-1, McClure Mountain, Emerald, and Durango) were evaluated to assess their long-term stability and to verify the reproducibility and reliability of the analytical protocol.

NW-1. NW-1 apatite was separated from a carbonatite sample collected from the Prairie Lake alkaline–carbonatite complex, Ontario, Canada[31]. Numerous geochronological studies have been carried out on this complex[32]. For example, two samples of baddeleyite from the carbonatite yield U–Pb ages of 1157.2 ± 2.3 Ma (2s, n=25) and 1158.2 ± 3.8 Ma (2s, n=35), identical to the age of 1163.6 ± 3.6 Ma (2s, n=35) obtained for baddeleyite from the iolite using SIMS [33]. Meanwhile the $^{207}Pb/^{206}Pb$ age of NW-1 apatite was 1155.3 ± 5.8 (2s, n=9/10) by ID-TIMS[33]. Recently, the $^{207}Pb/^{206}Pb$ age of PL57 Ti-bearing andradite was 1156.2 ± 2.4 (2s, n=10/12) by ID-TIMS [32]. The obtained $^{207}Pb/^{206}Pb$ ages were 1160

± 36 Ma (2s, n=33) by SIMS[6]. As summarized by Li et al.[32], the best-estimated age of the Prairie Lake alkaline–carbonatite complex is 1155 ± 5 Ma, representing a synthesis of multiple independent datasets [32-36].

NW-1 apatite displays a wide range of U concentrations, from 29 to 527 ppm. Common Pb contents are very low, with the mean f_{206} values between 0.5% and 3.2%. On the Tera–Wasserburg concordia diagram, both the lower-intercept age defined by 22 analytical spots (Session 1, Table S1) and the weighted mean $^{206}Pb/^{238}U$ age corrected using the ^{207}Pb method yield an age of 1164 ± 12 Ma (Table 2).

Long-term replicate analyses conducted over the past five years yield lower-intercept ages ranging from 1145 ± 13 Ma (2s, n=14) to 1172 ± 13 Ma (2s, n=26), despite substantial variation in U contents (28.6–380 ppm; Table 2; Table S1). When all 195 analyses are combined, the resulting lower-intercept age is 1157 ± 5 Ma (MSWD = 0.99; Fig. 1a, 1b), agree well with the recommended age using ID-TIMS by Wu *et al.*[33]

McClure Mountain. The McClure Mountain complex is a suite of ultramafic to silica-undersaturated alkaline igneous intrusions located in the Wet Mountains region of Colorado, USA[37,38]. U–Pb ID–TIMS dating of zircon from the McClure Mountain complex yielded an age of 523.98 ± 0.12 Ma (MSWD = 1.4)[39]. Apatite from the same locality was also dated by ID–TIMS using a three-dimensional total Pb–U isochron approach. After correction for common Pb, a $^{207}Pb/^{235}U$ cooling age of 523.51 ± 1.47 Ma (MSWD = 2.1) was obtained [39]. Subsequently, McClure Mountain apatite has been widely used as a reference material for LA-ICP-MS apatite U–Pb dating. The obtained intercept U-Pb ages by laser were 521.2 ± 6.2 Ma (2s, n=160)[7], 524.5 ± 3.7 (2s, n=33)[5], 516.3 ± 9.0 (2s, n=105)[16] and 526.1 ± 9.0 (2s, n=20;)[40], respectively.

In single analytical session, McClure Mountain apatite exhibits U concentrations ranging from 6.7 to 39.8 ppm, accompanied by variable common Pb proportions (f_{206} = 4.5–39.2%). The lower-intercept age defined by 27 analytical spots (S1) is 523.7 ± 6.6 Ma, and the corresponding ^{207}Pb-corrected weighted mean $^{206}Pb/^{238}U$ age is 523.1 ± 6.0 Ma (Table 2; Table S1). Replicate analyses conducted over five sessions show a broader range of U concentrations (8.0–40.5 ppm). When all replicated data are combined, the resulting lower-intercept age is 519.5 ± 2.0 Ma (2s, n=90, MSWD = 0.93; Fig. 1c), and the corresponding ^{207}Pb-corrected weighted mean $^{206}Pb/^{238}U$ age is 518.8 ± 2.2 Ma (2s, n=90, MSWD = 0.77; Fig. 1d).

Emerald. Emerald apatite is derived from the mid-Cretaceous composite Emerald Lake pluton exposed in the Yukon Territory, northern Canadian Cordillera. Detailed petrological and geochemical investigations of this pluton were carried out by Coulson *et al.*[41]. In the combined U–Pb and $^{40}Ar/^{39}Ar$ geochronological study of the Emerald Lake pluton by Coulson *et al.* [41], the oldest age was obtained from zircon U–Pb dating of syenite (94.5 ± 0.2 Ma), whereas the youngest age was derived from titanite U–Pb dating of granite (92.2 ± 0.9 Ma). More recently, the $^{206}Pb/^{238}U$ age of Emerald apatite was first reported as 95.18 ± 0.10 (2s, n=5) by ID-TIMS[42].

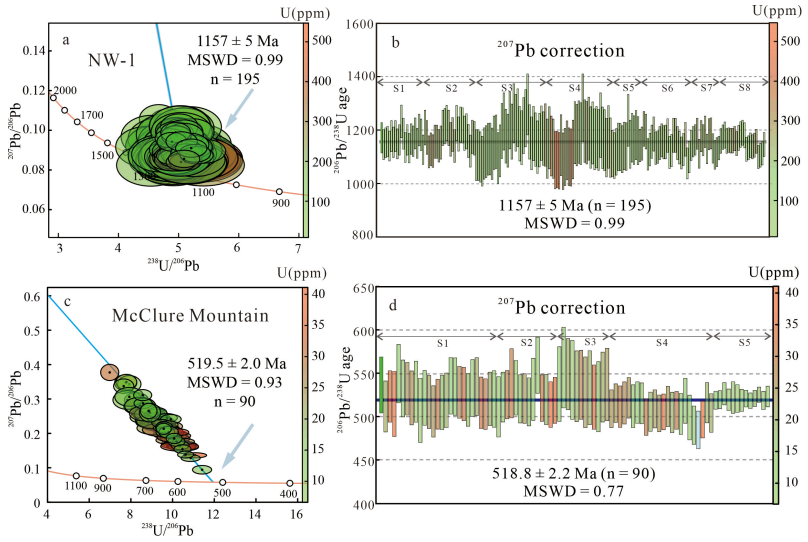

Fig. 1 LA-SF-ICP-MS U–Pb data of apatite samples NW-1 (a, b) and McClure Mountain (c, d). The Tera–Wasserburg diagram and the ^{207}Pb corrected weighted average $^{206}Pb/^{238}U$ ages are shown. The blue discordia lines in the Terra–Wasserburg diagrams are forced through a pre-determined $^{207}Pb/^{206}Pb$ for every sample. The $^{207}Pb/^{206}Pb$ values of the samples were estimated using the two-stage crustal Pb model proposed by Stacey and Kramers (1975) [9]. Error bars in the insets are at the 2s level.

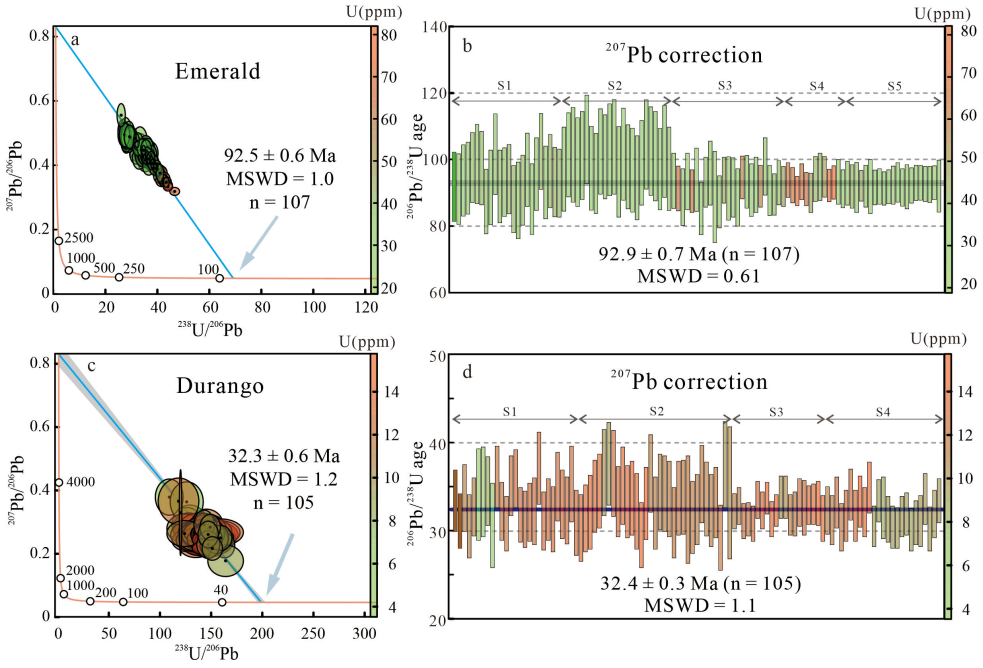

Fig. 2 LA-SF-ICP-MS U–Pb data of apatite samples Emerald (a, b) and Durango (c, d). The Tera–Wasserburg diagram and the ^{207}Pb corrected weighted average ^{206}Pb/^{238}U ages are shown. The blue discordia lines in the Terra–Wasserburg diagrams are forced through a pre-determined ^{207}Pb/^{206}Pb for every sample. The ^{207}Pb/^{206}Pb values of the samples were estimated using the two-stage crustal Pb model proposed by Stacey and Kramers (1975)[9]. Error bars in the insets are at the 2s level.

Emerald apatite contains high proportions of common Pb, with f_{206} values ranging from 34.0% to 63.9%, while U concentrations show relatively limited variation (18.5–79.6 ppm). For 24 analytical spots (S1) measured in a single session, the lower-intercept age obtained from the Tera–Wasserburg concordia diagram is 93.5 ± 2.1 Ma, and the corresponding ^{207}Pb-corrected weighted mean ^{206}Pb/^{238}U age is 93.5 ± 2.2 Ma (Table 2). Long-term replicate analyses conducted over four analytical sessions yield U concentrations ranging from 18.5 to 79.5 ppm (Table 2; Table S1). When all 107 analyses are combined, the resulting lower-intercept age is 92.5 ± 0.6 Ma (MSWD = 1.0; Fig. 2a, 2b), differing by less 2% from new ID-TIMS U–Pb age of Emerald reported by [42].

Durango. Durango apatite is a distinctive yellowish-green fluorapatite from the Cerro de Mercado open-pit iron mine, located in the northern suburbs of Durango City, Mexico[43,44]. Durango apatite occurs as coarse, ultra-large crystals and is widely used as a reference material for apatite fission track dating, (U–Th)/He dating, electron microprobe analyses and laser Sr-Nd measurement[8]. More recently, the ^{206}Pb/^{238}U age of Durango apatite was first reported as 32.29 ± 0.12 (2s, n=14) by ID-TIMS after correction of excess ^{206}Pb form Th-disequilibrium using a Th/U$_{melt}$ of 3.5 ± 1[10].

Durango apatite exhibits low and homogeneous U concentrations, ranging from 8.9 to 9.9 ppm in a single analytical session, whereas f_{206} values show relatively large variability, from 16.6% to 31%. For 27 analytical spots (S1), the ^{207}Pb-corrected weighted mean ^{206}Pb/^{238}U age is 32.8 ± 0.7 Ma, while the lower-intercept age on the Tera–Wasserburg diagram is 32.9 ± 0.7 Ma (Table 2; Table S1). Long-term replicate analyses across four analytical sessions, comprising 105 spots, yield a combined lower-intercept age of 32.3 ± 0.6 Ma (MSWD = 1.2; Fig. 2c, 2d), with U concentrations ranging from 3.5 to 15.2 ppm. Compared with the recommended age of 32.29 ± 0.12 Ma[10], the age discrepancies for single-session and combined datasets are 1.5% and 0.6%, respectively, highlighting the sensitivity of in situ U–Pb dating to high common Pb proportions and low U content in this sample.

Otter Lake. The Otter Lake area, Quebec, is located north of the Bancroft terrane within the Grenville orogen, at the boundary between the medium-grade metasedimentary belt and the medium-grade gneiss belt[45]. Barfod *et al.*[46] applied the ^{207}Pb/^{206}Pb step-leaching method to these apatites and obtained an isochron age of 913 ± 7 Ma (MSWD = 0.24) from the ^{207}Pb/^{204}Pb–^{206}Pb/^{204}Pb isotope diagram. Inductively coupled plasma mass spectrometry (ICP-MS) analyses yielded concentrations of 74 ppm Pb, 722 ppm Th, and 92 ppm U for the Otter Lake apatite[46]. The obtained intercept U-Pb ages by laser were 910 ± 13 Ma (2s, n=36)[47] and 933 ± 12 (2s, n=12)[5], respectively.

Otter Lake apatite exhibits moderate variability in U concentrations. Within a single analytical session (34 spots, S1), U contents range from 59 to 232 ppm, with corresponding f_{206} values of 1.8–3.9% (Table 2; Table S1). The resulting lower-intercept age of 915.1 ± 6.2 Ma is in excellent agreement with the ^{207}Pb-corrected

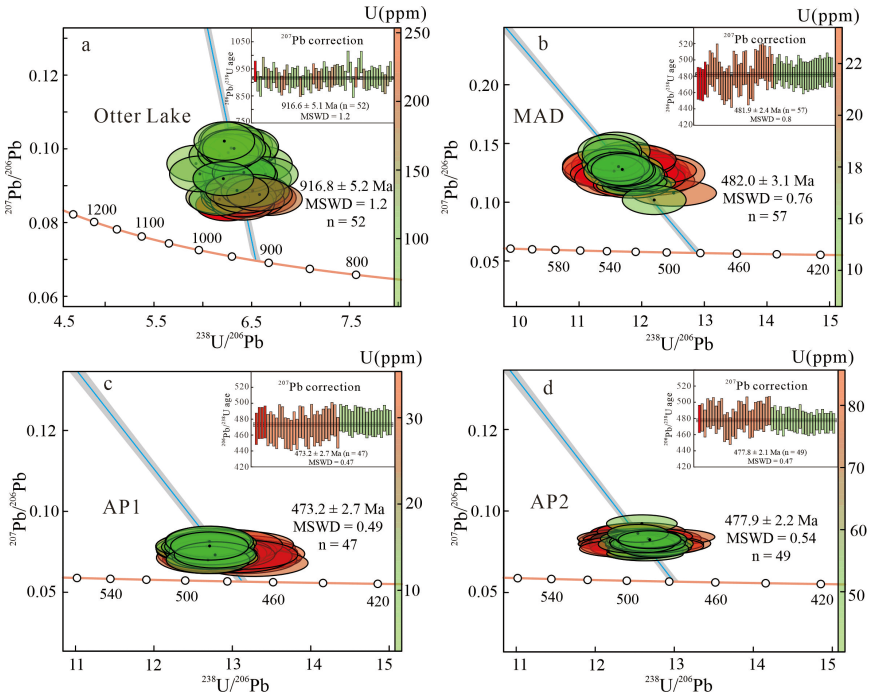

Fig. 3 LA-SF-ICP-MS U–Pb data of apatite samples Otter Lake (a), MAD (b), AP1 (c) and AP2 (d). The Tera–Wasserburg diagram and the ^{207}Pb corrected weighted average ^{206}Pb/^{238}U ages are shown. The blue discordia lines in the Terra–Wasserburg diagrams are forced through a pre-determined ^{207}Pb/^{206}Pb for every sample. The ^{207}Pb/^{206}Pb values of the samples were estimated using the two-stage crustal Pb model proposed by Stacey and Kramers (1975)[9]. Error bars in the insets are at the 2s level.

weighted mean ^{206}Pb/^{238}U age of 914.2 ± 6.2 Ma (Table 2). When data from two analytical sessions are combined (52 spots), the calculated lower-intercept age is 916.8 ± 5.2 Ma (MSWD = 1.2; Fig. 3a), with U concentrations spanning a wider range of 59–246 ppm (Table S1).

MAD. MAD (Madagascar) apatite is a fragment of a large, blue, gem-quality apatite crystal collected from the No. 1 deposit in Madagascar. ID–TIMS analyses were performed on four small fragments from another crystal from the same deposit. After correction for common Pb, a weighted mean ^{206}Pb/^{238}U age of 486.58 ± 0.85 Ma (2s, n=9) was obtained[7]. The obtained intercept U-Pb ages were 485.3 ± 4.9 Ma (2s, n=132) by LA-MC-ICP-MS from the same laboratory. The obtained intercept U-Pb ages were 474 ± 3 Ma (2s, n=40) by LA-Q-ICP-MS[11].

In two analytical session, MAD apatite exhibits relatively homogeneous U concentrations, ranging from 13.3 to 16.1 ppm, and low, stable proportions of common Pb (f_{206} = 5.6–10.7%) (Table 2; Table S1). The lower-intercept age defined by 57 analytical spots is 482.0 ± 3.1 Ma, and the corresponding ^{207}Pb-corrected weighted mean ^{206}Pb/^{238}U age is 481.9 ±2.4 Ma (Fig. 3b). These ages differ by only ~ 1.0% from the ID–TIMS age of 485.2 Ma reported by Thomson *et al.*[7], demonstrating the suitability of MAD apatite as a reliable reference material for in situ U–Pb analysis.

AP1 and AP2. AP1 and AP2 are gem-quality apatite crystals with uncertain provenance, although they are likely sourced from Madagascar. They have been widely used as reference materials for laser Sr and Nd isotope analyses and in situ U-Pb measurement has not multiply conducted in laboratory[8,48,49]. ID–TIMS analyses indicate that, after correction for common Pb, AP1 apatite yields a ^{206}Pb/^{238}U age of approximately 472.4 ± 2.5 Ma (2s, n=4) and the obtained intercept U-Pb ages were 472.0 ± 5.0 Ma (2s, n=20) by LA-Q-ICP-MS[50].

Both apatites contain extremely low and negligible amounts of common Pb, with f_{206} values ranging from 2.5% to 3.7% for AP1 and from 1.7% to 3.2% for AP2 (Table S1). Their U–Pb ages are essentially identical. For AP1, the lower-intercept age and the ^{207}Pb-corrected weighted mean ^{206}Pb/^{238}U age are both 473.2 ± 2.7 Ma (Fig. 3c). For AP2, the corresponding ages are 477.9 ± 2.2 Ma and 477.8 ± 2.1 Ma, respectively (Fig. 3d).

Despite their similar ages and common Pb characteristics, AP1 and AP2 differ markedly in U concentration. AP1 contains significantly lower U (16.9–32.3 ppm) than AP2 (42.3–84.2 ppm). This contrast in U abundance makes AP1 more suitable for applications requiring higher signal intensity, whereas AP2 is better suited as a secondary reference material with lower U concentrations.

Elemental contents and ratios. Variations in Th and U concentrations, as well as common Pb fractions, for the eight apatite samples analyzed are illustrated in Fig. 4. Uranium concentrations

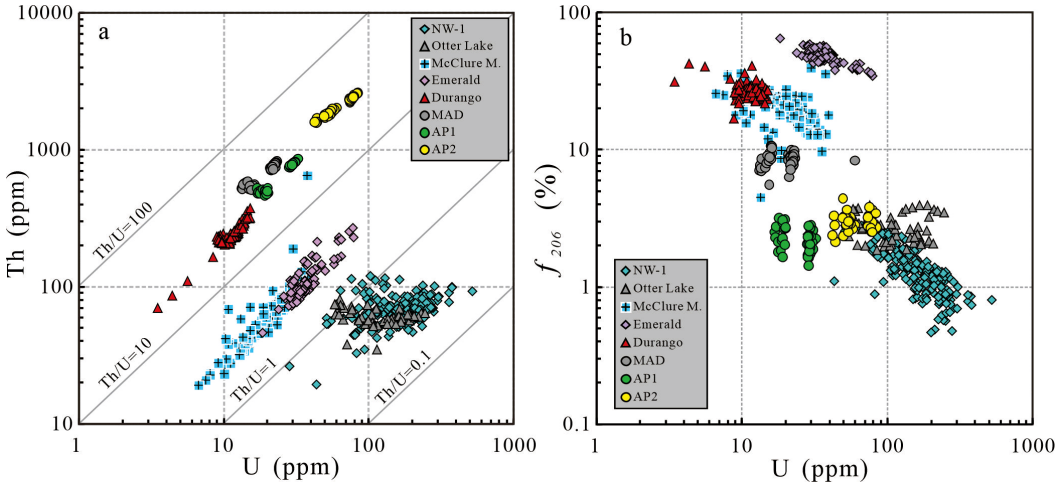

Fig. 4 (a) Comparison between U and Th concentrations in apatite. (b) Comparison between U concentrations and f_{206} in apatite (The f_{206} value represents the percentage of common ^{206}Pb in total ^{206}Pb of the analyzed apatite samples.)

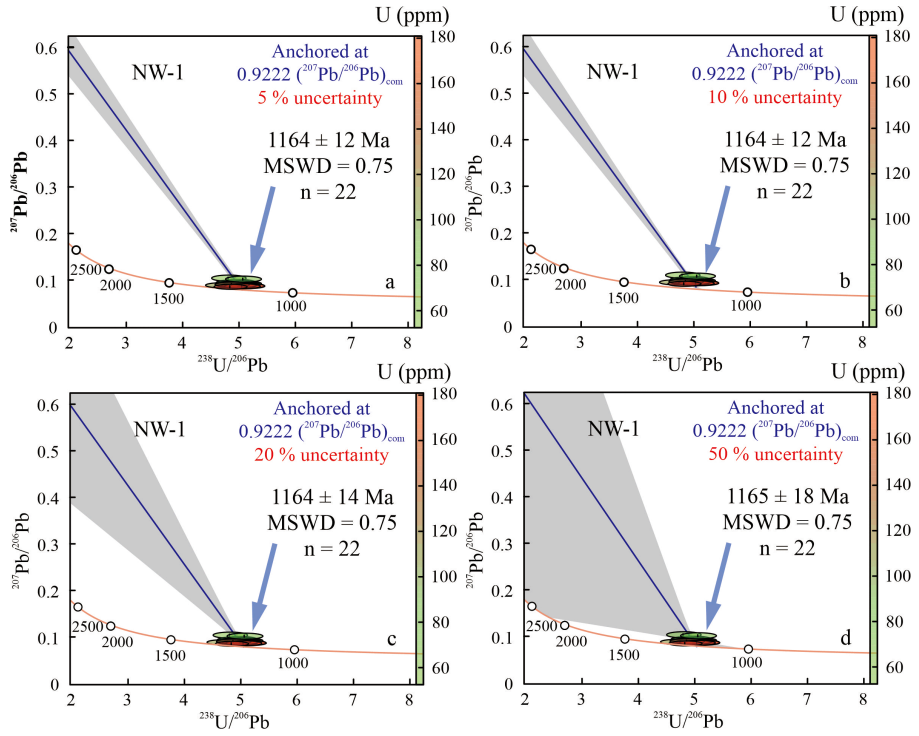

Fig. 5 The influence of different uncertainty levels (5%, 10%, 20%, 50%) of common Pb anchoring on the in situ U-Pb dating of apatite samples with low f_{206} values (NW-1, f_{206}~4.2%).

are generally low, ranging from 5 to 400 ppm. Among them, McClure Mountain, Durango, MAD and AP1 apatites exhibit particularly low U contents (<20 ppm). Thorium concentrations span a much wider range, from 20 to 2000 ppm. AP2 is characterized by exceptionally high Th contents (>1500 ppm), whereas Otter Lake, AP1, MAD, and display moderate Th concentrations (Table S1). In contrast, NW-1, McClure Mountain, Emerald, and Durango contain relatively low Th contents. The Th/U ratios of all apatite samples vary between 0.1 and 100. Notably, four samples (Durango, MAD, AP1, and AP2) show highly consistent and homogeneous Th and U concentrations (Fig 4a). Overall, common Pb contents are low across the dataset; however, the two Cenozoic samples, Emerald and Durango, exhibit relatively higher common Pb fractions. Comparative analysis indicates that Th

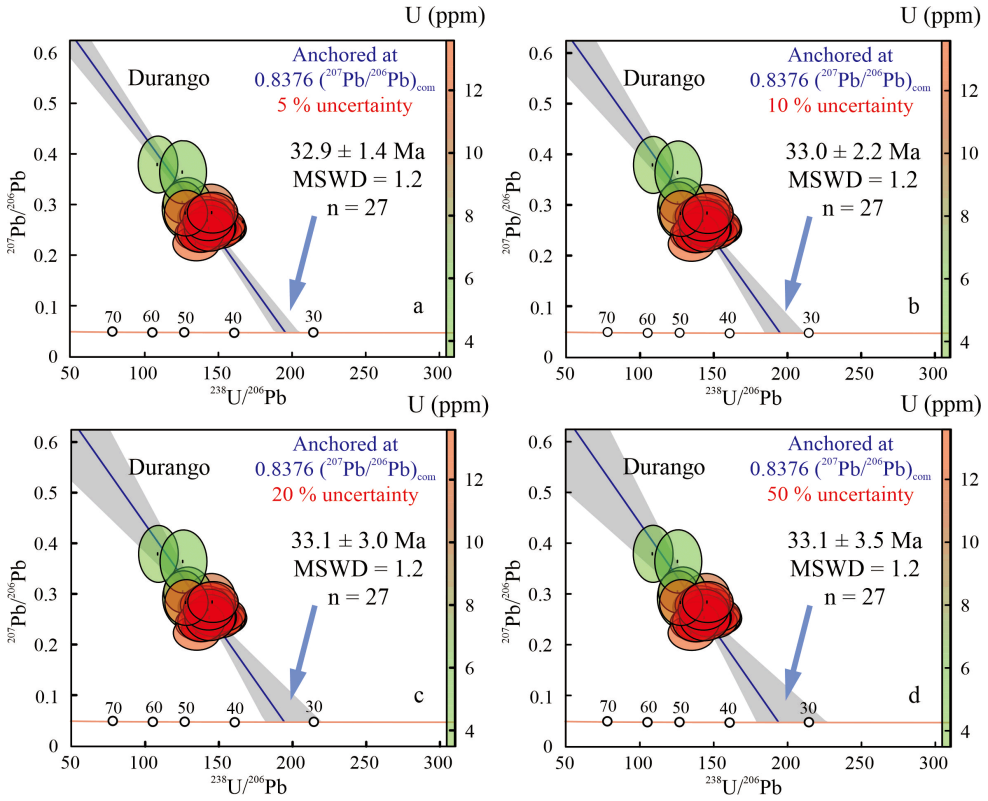

Fig. 6 The influence of different uncertainty levels (5%, 10%, 20%, 50%) of common Pb anchoring on the in situ U-Pb dating of apatite samples with medium f_{206} values (Emerald, f_{206} ~27%).

concentrations display an approximately positive covariation with U concentrations, whereas the variation in $f_{(206)}$ is generally inversely correlated with U content (Fig. 4b).

DISCUSSION

Impact of common Pb components on dating results. Common Pb represents one of the primary sources of uncertainty in U–Pb dating. Apatite typically contains low U concentrations and is therefore highly susceptible to the incorporation of common Pb. Consequently, reliable estimation and correction of common Pb are critical for ensuring accurate apatite U–Pb age determinations[5-7,15]. To assess the impact of common Pb components on dating results, we compared U–Pb ages obtained under anchored common Pb with uncertainty—for three apatite samples in the single analytical session (S1) with contrasting common Pb fractions ($f_{(206)}$): NW-1, Durango, and Emerald (Figs. 5–7; Table S1).

For NW-1, which exhibits the lowest common Pb fraction, anchoring the common Pb composition with varying levels of uncertainty yields consistent lower-intercept ages. The calculated ages are 1164 ± 12 Ma (5% uncertainty; Fig. 5a), 1164 ± 12 Ma (10%; Fig. 5b), 1164 ± 14 Ma (20%; Fig. 5c), and 1165 ± 18 Ma (50%; Fig. 5d). The resulting age discrepancies are negligible, indicating that common Pb uncertainty has a minimal influence on samples with very low f_{206}.

For Durango apatite, which contains a moderate proportion of common Pb, the lower-intercept ages show slightly greater sensitivity to common Pb uncertainty. The calculated ages vary from 32.9 ± 1.4 Ma (5%; Fig. 6a) to 33.0 ± 2.2 Ma (10%; Fig. 6b), 33.1 ± 3.0 Ma (20%; Fig. 6c), and 33.1 ± 3.5 Ma (50%; Fig. 6d). Correspondingly, the relative age discrepancy decreases from 2.3% to 1.6%, suggesting that anchoring common Pb can moderately stabilize age estimates for samples with intermediate common Pb contents.

In contrast, Emerald apatite, characterized by a high common Pb fraction (~50%), exhibits pronounced age variations under different anchoring uncertainties. The lower-intercept age shifts from 92.4 ± 9.9 Ma (5%; Fig. 7a) to 89 ± 20 Ma (10%; Fig. 7b), 78 ± 40 Ma (20%; Fig. 7c), and 63 ± 58 Ma (50%; Fig. 7d). These results clearly demonstrate that anchoring the common Pb composition exerts a significant control on the U–Pb age of apatites with high common Pb proportions.

In summary, rational anchoring of common Pb components facilitates more accurate and stable age determinations, particularly

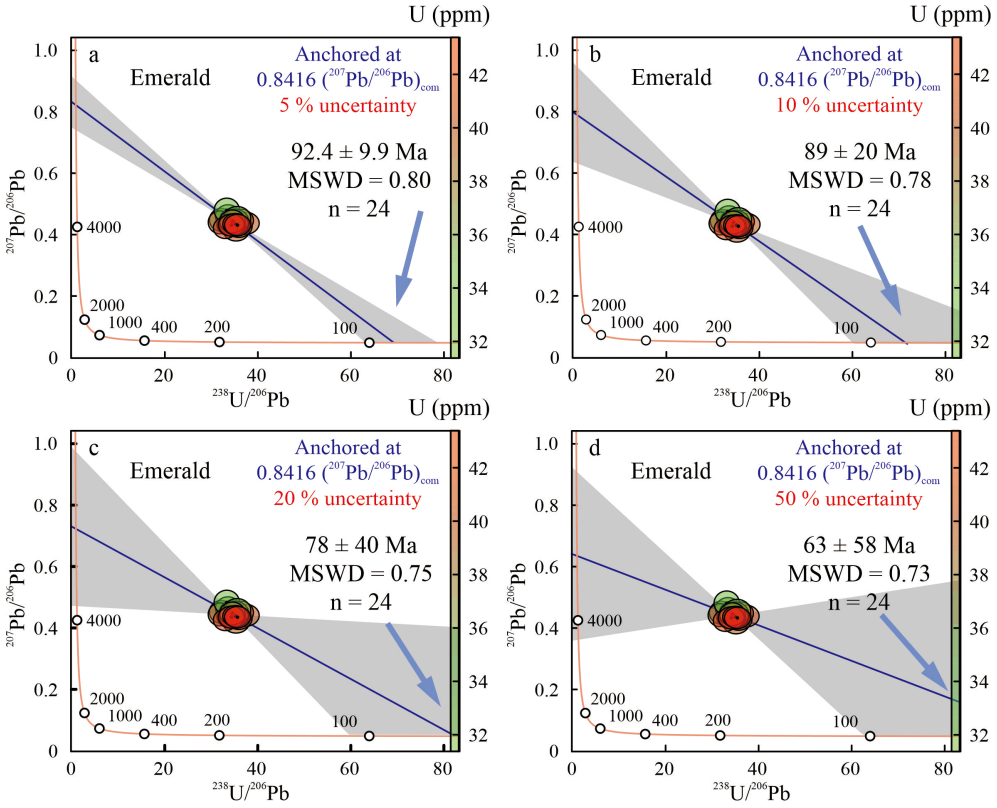

Fig. 7 The influence of different uncertainty levels (5%, 10%, 20%, 50%) of common Pb anchoring on the in situ U-Pb dating of apatite samples with high f_{206} values (Emerald, f_{206}~48%).

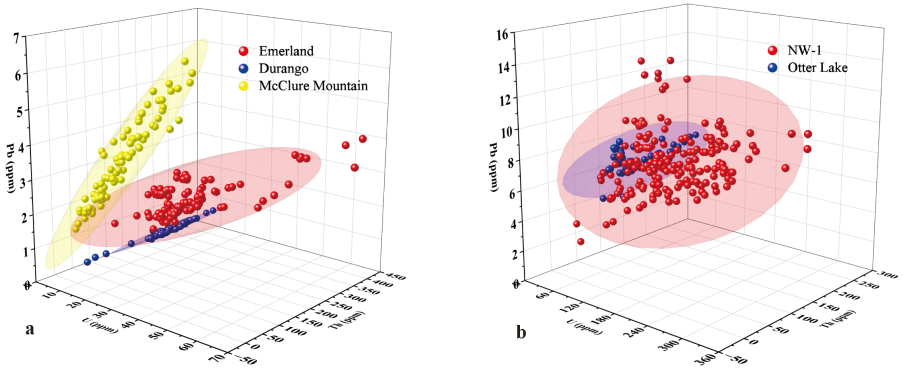

Fig. 8 U-Th-Pb contents of Emerald, Durango, McClure Mountain (a) and NW-1, Otter Lake (b); The shaded area represents the 95% confidence interval.

for samples with high f_{206} values, where the effect is most pronounced. Additionally, anchoring the upper intercept can reduce age uncertainty to some extent.

Therefore, during Tera–Wasserburg (T–W) concordia fitting, appropriate anchoring of the upper intercept can partially mitigate fitting errors arising from uncertainties in common Pb composition, reduce lower-intercept age drift caused by data scatter, and suppress the influence of open-system behavior (e.g., Pb incorporation or loss) on age calculations. This approach helps constrain the lower-intercept age closer to its true geological value. However, for ancient samples with low f_{206} values—where radiogenic ^{206}Pb dominates and common Pb interference is minimal—the reliance on external constraints is reduced. In such cases, an inaccurately preset upper-intercept value may introduce over-correction, leading to deviations from the true age. Consequently, careful selection of

Table 3. Compilation of U-Pb age results in this work and literature for apatite reference materials

Samples	Pb (ppm)	CV (%)	Th (ppm)	CV (%)	U (ppm)	CV (%)	U-Pb age (±2s) (Ma)	^{207}Pb corr. age (±2s) (Ma)	n	Methods	References
NW-1	8.13 ± 1.88	23	70.5 ± 17.0	24	171 ± 75	43	1156 ± 4	1156 ± 36	256	LA-SF-ICP-MS	This study
							1155.3 ± 4.4#	1168.3 ± 4.4	9	ID-TIMS	Wu *et al.* [51]
			~ 38		18 ~ 162		1160 ± 36		33	SIMS	Li *et al.*[6]
McClure M.	3.63 ± 1.19	32	60.6 ± 25.5	42	19.9 ± 7.7	38	519.5 ± 4.0	518.8 ± 4.4	90	LA-SF-ICP-MS	This study
							526.1 ± 9.0	524.2 ± 3.9	20	LA-ICP-MS/MS	Sarah et al., 2020
			~ 38		~ 13		516.3 ± 9.0		105	LA-Q-ICP-MS	Thompson *et al.*[16]
	6.7		58		19.6		524.5 ± 3.7	524.6 ± 3.2	33	LA-Q-ICP-MS	Chew *et al.* [4]
							521.2 ± 6.2		160	LA-MC-ICP-MS	Thomson *et al.*[7]
							523.51 ± 1.47		7	ID-TIMS	Schoene *et al.*[39]
Emerald	2.72 ± 0.55	20	113 ± 42	37	38.3 ± 10.9	29	92.5 ± 0.6	92.9 ± 0.7	107	LA-SF-ICP-MS	This study
								95.18 ± 0.10	5	ID-TIMS	Apen *et al.*[42]
			106		41		92.9 ± 2.2		77	LA-Q-ICP-MS	Thompson *et al.*[16]
	3.22		122		47.2		92.5 ± 3.3	90.5 ± 3.1	33	LA-SF-ICP-MS	Chew *et al.*[5]
Durango	0.66 ± 0.14	22	247 ± 45	18	11.7 ± 2.0	17	32.3 ± 0.6	32.4 ± 0.3	105	LA-SF-ICP-MS	This study
	0.094		443		30.9			32.1 ± 0.6	36	LA-Q-ICP-MS	Tu *et al.*[47]
							31.5 ± 0.9	31.1 ± 0.9	40	LA-Q-ICP-MS	Duan *et al.*[11]
								32.29 ± 0.12	14	ID-TIMS	Paul *et al.*10
			~ 269		~ 12			30.87 ± 0.82	77	LA-Q-ICP-MS	Thompson *et al.*[16]
	0.3		270		14.5		31.97 ± 0.59	32.20 ± 0.51	36	LA-Q-ICP-MS	Chew *et al.*[4]
			~ 180		8.4 ~ 12.3		32 ± 2	31 ± 2	18	SIMS	Li *et al.*[6]
								32.2 ± 5.3	10	LA-MC-ICP-MS	Thomson *et al.*[7]
	1.00		556		31.7		32.3 ± 2.4	30.6 ± 2.3	19	LA-SF-ICP-MS	Chew *et al.*[55]
Otter Lake	6.84 ± 0.86	13	60.5 ± 8.4	14	127 ± 51	40	915 ± 3	915 ± 3	110	LA-SF-ICP-MS	This study
	1.15		300		51.1		910 ± 13		36	LA-Q-ICP-MS	Tu *et al.*[47]
	96.1		1487		195		933 ± 12	932 ± 12	12	LA-SF-ICP-MS	Chew *et al.*[55]
	74		722		92		913 ± 7		5	ID-TIMS	Barfod *et al.*[46]
MAD	23.3 ± 9.1	39	673 ± 117	18	18.9 ± 3.7	19	483.2 ± 3.2	483.2 ± 3.3	25	LA-SF-ICP-MS	This study
							473 ± 3	474 ± 3	40	LA-Q-ICP-MS	Duan *et al.*[11]
								486.58 ± 0.85	9	ID-TIMS	Thomson *et al.*[7]
								485.3 ± 4.9	132	LA-MC-ICP-MS	Thomson *et al.*[7]
AP1	23.5 ± 8.3	36	676 ± 144	21	25.5 ± 5.4	21	476.8 ± 3.5	477.1 ± 7.6	18	LA-SF-ICP-MS	This study
								472.4 ± 2.5	4	ID-TIMS	Zhou [50]
AP2	35.2	45	1758	14	51.0	20	476.5 ± 2.7	476.3 ± 2.7	23	LA-SF-ICP-MS	This study
							472.0 ± 5.0	473.0 ± 6.0	20	LA-Q-ICP-MS	Zhou [50]

common Pb values is essential when applying anchored age corrections.

Evaluation of long-term stability and homogeneity of apatite reference materials. This study presents long-term replicate analytical data for four widely used reference materials in apatite U–Pb geochronology: NW-1, McClure Mountain, Emerald, and Durango. The obtained U–Pb ages are in good agreement with their recommended reference ages (Table 2; Table S1), thereby confirming the long-term analytical stability of these apatite reference materials.

In addition to age reproducibility, elemental homogeneity is a critical prerequisite for obtaining reliable in situ microanalytical U–Pb ages. Reference materials with homogeneous elemental distributions can effectively minimize systematic uncertainties associated with variations in laser ablation behavior, elemental fractionation, and instrumental mass bias[51]. Moreover, geological studies commonly require cross-validation of analytical results among different laboratories, for which reference materials with well-characterized and homogeneous elemental compositions provide essential benchmarks to ensure interlaboratory comparability[11,15,52].

We further evaluated the variability of U, Th and Pb concentrations among the analyzed reference materials. The results show that Emerald, Durango, Durango, McClure Mountain, NW-1 and Otter Lake apatites exhibit favorable homogeneity. As shown in Fig. 8, most data points for U, Th and Pb concentrations fall within the confidence interval, with only a few outliers outside the interval, suggesting a good overall fitting performance and minor dispersion in individual spots. A comparative evaluation reveals that Durango displays the best overall homogeneity (low CV), whereas McClure Mountain and Emerald show relatively poorer homogeneity (high coefficient of variation) (Table 3). MAD, AP1, and AP2 are homogeneous in Th and U contents, but exhibit relatively large fluctuations in Pb. In contrast, NW-1 and Otter Lake show relatively dispersed U concentrations (Table 3, Fig. 8). Overall, the elemental concentrations from replicate analyses of these reference materials vary within a narrow range, indicating a high degree of internal compositional uniformity.

Matrix matching and applicability of reference materials. In situ U–Pb dating of apatite requires appropriate matrix matching to ensure the accuracy, reliability, and comparability of analytical results. During in situ analyses of unknown samples, laser ablation behavior, elemental fractionation processes, and related physicochemical effects can be highly variable and often more complex than those observed in reference materials. Consequently, in practical geochronological applications, careful consideration must be given to the suitability and applicability of different apatite reference materials.

For example, the U–Pb systems of some ancient geological samples may be susceptible to late-stage modification, resulting in Pb that is predominantly radiogenic. Owing to its extremely low common Pb content and relatively high U concentration, NW-1 apatite has therefore been widely used as a reference material for dating Mesoarchean samples[6,33]. Otter Lake apatite, which is hosted at the boundary between a medium-grade metasedimentary belt and a medium-grade gneiss belt and experienced high-amphibolite-facies metamorphism, exhibits excellent matrix compatibility with certain low-U metamorphic apatite. As a result, it achieves high analytical accuracy in such applications [5,53]. Madagascar (MAD) apatite, characterized by excellent U–Pb isotopic homogeneity, a stable Th/U ratio, and moderate U contents, has become an ideal reference material for Paleozoic apatite U–Pb dating[4,7,11,54]. Its high degree of homogeneity ensures reliable in situ analytical results, and in some cases allows direct calibration without the need for common Pb correction[56,57]. Durango apatite represents the youngest available reference material for apatite U–Pb geochronology and is also a globally recognized benchmark for (U–Th)/He thermochronology and in situ analytical studies. It is therefore particularly valuable for investigations of Cenozoic magmatic–hydrothermal systems, orogenic exhumation, and cooling histories[15].

In practical applications, the major- and trace-element compositions (especially U, Th, Pb, and potential interfering elements), as well as the approximate age range of unknown samples, can usually be constrained prior to analysis. The most appropriate reference material should therefore be selected by integrating multiple criteria, including age compatibility, elemental concentrations and ratios, geological background, and relevant physicochemical properties, to minimize age bias and correction uncertainties. Although existing apatite U–Pb reference materials now collectively cover a broad range of ages and analytical techniques, there remains a shortage of truly high-quality reference materials[15]. Individual reference materials inevitably have inherent limitations; consequently, the combined use of multiple reference materials for cross-calibration and mutual verification represents an effective strategy for improving the robustness and reliability of apatite U–Pb dating results.

CONCLUSION

This study presents in situ apatite U–Pb dating results obtained by LA–SF–ICP–MS for apatite reference materials and samples spanning an age range of approximately 1156–32 Ma. The resulting in situ U–Pb ages are consistent, within analytical uncertainties, with corresponding ID-TIMS ages or previously reported reference values, demonstrating the accuracy and robustness of the established analytical protocol. Age calculations based on Tera–Wasserburg concordia diagrams indicate that rational anchoring of the common Pb component significantly

improves age accuracy, particularly for samples with high common Pb fractions, whereas samples with low common Pb contents show reduced dependence on external constraints. Long-term replicate analyses further confirm the stability and elemental homogeneity of several widely used apatite reference materials, with McClure Mountain, Emerald, and Durango exhibiting relatively uniform U–Pb concentrations and U–Pb ages consistent with their reference values. Although multiple apatite reference materials are currently available for U–Pb geochronology, their applicability must be carefully evaluated in practical geological contexts by considering age compatibility, elemental compositions, geological background, and matrix effects. Among the investigated materials, NW-1 apatite, characterized by high U contents and minimal common Pb, is recommended as a primary reference material, whereas AP1 and AP2 are more suitable as secondary reference materials. Overall, this study clarifies the appropriate application of different apatite reference materials and provides a practical framework for matrix matching and multi-reference material cross-calibration in in situ apatite U–Pb geochronology.

ASSOCIATED CONTENT

The supporting information (Tables S1) is available at https://www.at-spectrosc.com.

AUTHOR INFORMATION

Yue-Heng Yang received his B.S. degree from China University of Geosciences (Wuhan) in 1995 and his Ph.D. degree from the Institute of Geology and Geophysics, Chinese Academy of Sciences (IGGCAS) in 2007. He is currently a Professor-level Senior Engineer and doctoral supervisor at the Institute of Geology and Geophysics, Chinese Academy of Sciences. He has published more than 40 SCI papers as first or corresponding author and holds four authorized invention patents. In addition, he has co-authored over 300 scientific papers, which have received more than 22,000 citations, with an H-index of 84 according to Google Scholar. His research has long focused on the development and application of experimental techniques in (multi-collector) plasma mass spectrometry. His work particularly emphasizes laser microbeam in-situ (MC)-ICP-MS U-Th-Pb geochronology and Sr-Nd-Hf isotope analytical methods and their applications to geological materials. He was awarded the National Science Fund for Distinguished Young Scholars in 2015 and was selected as a National Leading Talent in Science and Technology Innovation (4th batch) by the Organization Department of the CPC Central Committee in 2019. He currently serves as a member of the editorial boards of *Science China Earth Sciences* and *Atomic Spectroscopy*.

Corresponding Author

* Y. H. Yang

Email address: yangyueheng@mail.iggcas.ac.cn

Notes

The authors declare no competing financial interest.

ACKNOWLEDGMENTS

This work was financially supported by the Deep Earth Probe and Mineral Resources Exploration-National Science and Technology Major Project (2025ZD1005300) and Natural Science Foundation of China (42430105 and 42573030). Weare also grateful to two reviewers for insightful comments that significantly improved this manuscript.

REFERENCES

1. D. J. Cherniak, W. A. Lanford, and F. J. Ryerson, *Geochim. Cosmochim. Acta*, 1991, **55**, 1663–1673. https://doi.org/10.1016/0016-7037(91)90137-T
2. Y. Amelin and A. N. Zaitsev, *Geochim. Cosmochim. Acta*, 2002, **66**, 2399–2419. https://doi.org/10.1016/S0016-7037(02)00831-1
3. K. R. Chamberlain and S. A. Bowring, *Chem. Geol.*, 2001, **172**, 173–200. https://doi.org/10.1016/S0009-2541(00)00242-4
4. D. M. Chew, J. A. Petrus, and B. S. Kamber, *Chem. Geol.,* 2014, **363**, 185–199. https://doi.org/10.1016/j.chemgeo.2013.11.006
5. Chew, D. M., Sylvester, P. J., and Tubrett, M. N., *Chem. Geol.*, 2011, **280**, 200–216. https://doi.org/10.1016/j.chemgeo.2010.11.010
6. Q. L. Li, X. H. Li, F. Y. Wu, Q. Z. Yin, H. M. Ye, Y. Liu, G. Q. Tang, and C. L. Zhang, *Gondwana Res.*, 2012, **21**, 745–756. https://doi.org/10.1016/j.gr.2011.07.008
7. S. N. Thomson, G. E. Gehrels, J. Ruiz, and R. Buchwaldt, *Geochem. Geophys. Geosyst.*, 2012, **13**, Q0AA21. https://doi.org/10.1029/2011GC003928
8. Y. H. Yang, F. Y. Wu, J. H. Yang, D. M. Chew, L. W. Xie, Z. Y. Chu, Y. B. Zhang, and C. Huang, *Chem. Geol.*, 2014, **385**, 35–55. https://doi.org/10.1016/j.chemgeo.2014.07.012
9. D. F. Xiang, Z. Y. Zhang, T. Zack, D. Chew, Y. H. Yang, L. Wu, and J. Hogmalm, Apatite U-Pb Dating with Common Pb Correction Using LA-ICP-MS/MS. Geostandards and Geoanalytical Research, 2021, **45**, 621–642. https://doi.org/10.1111/ggr.12404
10. A. N. Paul, R. A. Spikings, and S. P. Gaynor, *Chem. Geol.*, 2021, **586**, 120604 https://doi.org/10.1016/j.chemgeo.2021.120604
11. L. K. Duan, L. L. Zhang, D. C. Zhu, Y. H. Yang, J. C. Xie, Q. Wang, S. T. Wu, C. Huang, C. Li, W. T. Xu, S. Kamo, L. J. Xu, C. X. Pan, and G. H. Shi, *J. Anal. At. Spectrom.*, 2023, **35**, 1472–1481. https://doi.org/10.1039/d2ja00405d
12. F. E. Apen, S. P. Gaynor, B. Schoene, and J. M. Cottle, *Chem. Geol*, 2024, **661**, 12291.

https://doi.org/10.1016/j.chemgeo.2024.122191

13. T. Luo, and Z. C. Hu, *Earth Science*, 2022, **47**, 4122–4144. https://doi.org/10.3799/dqkx.2022.365
14. S. E. Gilbert and S. Glorie, *J. Anal. At. Spectrom.*, 2020, **35**, 1472–1481. https://doi.org/10.1039/D0JA00224K
15. T. Luo, H. L. Wang, S. B. Zhu, L. Y. Qing, and Z. C. Hu, *Rock and Mineral Analysis*, 2025, **44(01)**, 51–62. https://doi.org/10.15898/j.ykcs.202404070079
16. J. Thompson, S. Meffre, R. Maas, V. Kamenetsky, M. Kamenetsky, K. Goemann, K. Ehrig, and L. Danyushevsky, *J. Anal. At. Spectrom.*, 2016, **31**, 1206–1215. https://doi.org/10.1039/C6JA00048G
17. C. Lana, G. O. Goncalves, A. Mazoz, I. Buick, S. Kamo, R. Scholz, H. Wang, Y. H. Yang, H. Moreira, M. Babinski, and G. Queiroga, *Geostand. Geoanal. Res.*, 2022, **46**, 71-95. https://doi.org/10.1111/ggr.12413
18. M. Yang, R. L. Romer, Y. H. Yang, S. T. Wu, H. Wang, J. R. Tu, H. Y. Zhou, L. W. Xie, C. Huang, L. Xu, J. H. Yang, and F. Y. Wu, *Chem. Geol.*, 2022, **593**. https://doi.org/10.1016/j.chemgeo.2022.120754
19. M. Yang, Y. H. Yang, S. T. Wu, R. L. Romer, X. D. Che, Z. F. Zhao, W. S. Li, J. H. Yang, F. Y. Wu, L. W. Xie, C. Huang, D. Zhang, and Y. Zhang, *J. Anal. At. Spectrom.*, 2020, **35**, 2191–2203. https://doi.org/10.1039/d0ja00248h
20. Y. H. Yang, S. T. Wu, H. Wang, S. L. Kamo, Q. Ma, T. Liang, L. Xu, L. W. Xie, C. Huang, B. Wan, J. H. Yang, and F. Y. Wu, *J. Anal. At. Spectrom.*, 2025, **40**, 326–337. https://doi.org/10.1039/d4ja00290c
21. S. T. Wu, Y. H. Yang, N. M. W. Roberts, M. Yang, H. Wang, Z. W. Lan, B. H. Xie, T. Y. Li, L. Xu, C. Huang, L. W. Xie, J. H. Yang, and F. Y. Wu, *Sci. China-Earth Sci.*, 2022, **65**, 1146–1160. https://doi.org/10.1007/s11430-021-9907-1
22. S. T. Wu, Y. H. Yang, H. Wang, C. Huang, L. W. Xie, and J. H. Yang, *Atom. Spectrosc.*, 2020, **41**, 154–161. https://doi.org/10.46770/As.2020.04.003
23. N. J. Pearce, W. T. Perkins, J. A. Westgate, M. P. Gorton, S. E. Jackson, C. R. Neal, and S. P. Chenery, *Geostandards Newsletter*, 1997, **21**, 115–144. https://doi.org/10.1111/j.1751-908X.1997.tb00538.x
24. S. T. Wu, G. Wörner, K. P. Jochum, B. Stoll, K. Simon, and A. Kronz, *Geostand. Geoanal. Res.*, 2019, **43**, 567-584. https://doi.org/10.1111/ggr.12301
25. C. Paton, J. Hellstrom, B. Paul, J. Woodhead, and J. Hergt, *J. Anal. At. Spectrom.*, 2011, **26**, 2508–2518. https://doi.org/10.1039/c1ja10172b
26. C. Paton, J. Woodhead, J. Hellstrom, J. Hergt, and A. Greig, *Chem. Geol.*, 2010, **274**, 1–15. https://doi.org/10.1016/j.chemgeo.2010.03.014
27. P. Vermeesch, *Geosci. Front.*, 2018, **9**, 1479–1493. https://doi.org/10.1016/j.gsf.2018.04.001
28. J. Hiess, D. J. Condon, N. McLean, and S. R. Noble, *Science*, 2012, **335**, 1610-1614. https://doi.org/10.1126/science.1215507
29. J. S. Stacey and J. D. Kramers, *Earth Planet. Sci. Lett.*, 1975, **26**, 207–221. https://doi.org/10.1016/0012-821X(75)90088-6
30. J. Lin, Y. S. Liu, L. Y. Zhu, and W. Zhang, *Spectrochim. Acta B*, 2021, **177**, 106074. https://doi.org/10.1016/j.sab.2021.106074
31. Y. Sano, T. Oyama, K. Terada, and H. Hidaka, *Chem. Geol.*, 1999, **153**, 249–258. https://doi.org/Doi10.1016/S0009-2541(98)00163-6
32. D. F. Li, Y. Fu, P. Hollings, R. Mitchell, S. Zurevinski, S. Kamo, R. Q. Zhang, Y. Zhang, Q. F. Liu, J. L. Liao, Y. J. Liang, and X. M. Sun, *Contrib. Mineral. Petrol.*, 2022, **177**, 19. https://doi.org/10.1007/s00410-021-01884-4
33. F. Y. Wu, R. H. Mitchell, Q. L. Li, C. Zhang, and Y. H. Yang, *Geol. Mag.*, 2017, **154**, 217–236. https://doi.org/10.1017/S0016756815001120
34. I. S. Brandt, S. V., Rasskazov, A. V. Ivanov, L. Z. Reznitskii, and S. B. Brandt, *Isot. Environ. Health S.*, 2006, **42**, 189–201. https://doi.org/10.1080/10256010500502686
35. E. B. Salnikova, S. A. Sergeev, A. B. Kotov, S. Z. Yakovleva, R. H. Steiger, L. Z. Reznitskiy, and E. P. Vasil'ev, *Gondwana Res.*, 1998, **1**, 195–205. https://doi.org/10.1016/S1342-937x(05)70830-3
36. Y. H. Yang, F. Y. Wu, J. H. Yang, R. H. Mitchell, Z. F. Zhao, L. W. Xie, C. Huang, Q. Ma, M. Yang, and H. Zhao, *J. Anal. At. Spectrom.*, 2018, **33**, 231–239. https://doi.org/10.1039/c7ja00315c
37. D. R. Shawe and R. L. Parker, U.S. *Geol. Surv. Bull.*, 1967, **1251-A**, 1–20.
38. J. C. Olson, R. F. Marvin, R. L. Parker, and H. H. Mehnert, *US Geol. Surv. J. Res.*, 1997, **5**, 673–687.
39. B. Schoene and S. A. Bowring, *Contrib. Mineral. Petrol.*, 2006, **151**, 615–630. https://doi.org/10.1007/s00410-006-0077-4
40. S. E. Gilbert and S. Glorie, *J. Anal. At. Spectrom.*, 2020, **35**, 1472–1481. https://doi.org/10.1039/d0ja00224k
41. I. M. Coulson, M. E. Villeneuve, G. M. Dipple, R. A. Duncan, J. K. Russell, and J. K. Mortensen, *J. Volcanol. Geotherm. Res.*, 2002, **114**, 331–356. https://doi.org/10.1016/S0377-0273(01)00294-3
42. F. Apen, S. Gaynor, and B. Schoene, *Data in Brief*, 2025, **60**, 111464. https://doi.org/10.17632/34jn7b8m6z.2
43. J. I. Lyons, *Econ. Geol.*, 1988, **83**, 1886–1906. https://doi.org/10.2113/GSECONGEO.83.8.1886
44. F. W. McDowell, W. C. McIntosh, and K. A. Farley, *Chem. Geol.*, 2005, **214**, 249–263. https://doi.org/10.1016/j.chemgeo.2004.10.002
45. R. Kretz, J. L. Campbell, E. L. Hoffman, R. Hartree, and W. J. Teesdale, *J. Metamorph. Geol.*, 1999, **17**, 41–59. https://doi.org/10.1046/j.1525-1314.1999.00180.x
46. G. H. Barfod, E. J. Krogstad, R. Frei, and F. Albarède, *Geochim. Cosmochim. Acta*, 2005, **69**, 1847–1859. https://doi.org/10.1016/j.gca.2004.09.014
47. J. R. Tu, H. Y. Zhou, Y. R. Cui, G. Z. Li, J. Z. Geng, and J. Zhang, *Rock and Mineral Analysis*, 2024, **43**, 533-545. https://doi.org/10.15898/j.ykcs.202404170087
48. Y. H. Yang, J. F. Sun, L. W. Xie, H. R. Fan, and F. Y. Wu, *Chin. Sci. Bull.*, 2008, **53**, 1062–1070. https://doi.org/10.1007/s11434-008-0166-z
49. Y. H. Yang, F. Y. Wu, S. A. Wilde, X. M. Liu, Y. B. Zhang, L. W. Xie, and J. H. Yang, *Chem. Geol.*, 2009, **264**, 24–42. https://doi.org/10.1016/j.chemgeo.2009.02.011
50. Q. Zhou, PhD dissertation, Institute of Geology and Geophysics, CAS, 2013.
51. L. Wu, F. Wang, J. N. Shan, W. B. Zhang, W. B. Shi, and H. L. Feng, *Acta Petrol. Sin.*, 2016, **32**, 1891–1900. http://www.ysxb.ac.cn/en/article/id/aps_20160621
52. C. Huang, H. Wang, J. H. Yang, J. Ramezani, C. Yang, S. B. Zhang, Y. H. Yang, X. P. Xia, L. J. Feng, J. Lin, T. T. Wang, Q. Ma, H. Y. He, L. W. Xie, and S. T. Wu, *Geostand. Geoanal. Res.*, 2020, **44**, 103–123. https://doi.org/10.1111/ggr.12307
53. J. H. Metcalfe, R. A. Strachan, J. R. Darling, M. Fowler, G. Chapman, and J. Dunlop, *Journal of the Geological Society, J. Geol. Soc. London*, 2024, **181**, jgs2023-139. https://doi.org/10.1144/jgs2023-139

54. Y. S. Cheng, Z. B. Xu, H. F. Di, Z. W. Zhang, C. W. Mao, H. J. Tan, J. Z. Huang, F. C. Zhou, L. P. Zhang, J. F. Chen, and C. H. Wen, *Minerals*, 2022, **12**, 344. https://doi.org/10.3390/min12030344
55. D. W. Chew, M. G. Babechuk, N. Cogné, C. Mark, G. J. O'Sullivan, I. A. Henrichs, D. Doepke, and C. A. McKenna, *Chem. Geol.*, 2016, **435**, 35–48. https://doi.org/10.1016/j.chemgeo.2016.03.028
56. L. H. Zhao, X. C. Zhan, L. S. Zeng, M. Y. Hu, D. Y. Sun, and J. H. Yuan, *Rock and Mineral Analysis*, 2022, **41**, 744–753. https://doi.org/10.15898/j.cnki.11-2131/td.202202260035
57. S. He, D. F. Guo, J. Y. Cui, Z. W. Fan, G. F. Liu, and Y. Wu, *Uranium Geology*, 2021, **37**, 1121–1130. https://d.wanfangdata.com.cn/periodical/ykdz202106014